Low-Temperature Crystallization of Silicon Films Directly Deposited on Glass Substrates Covered with Yttria-Stabilized Zirconia Layers

Susumu Horita and Sukreen Hana

School of Materials Science, Japan Advanced Institute of Science and Technology, 1-1 Asahidai, Nomi, Ishikawa 923-1292, Japan

Si films were deposited at low temperatures on glass substrates covered with poly-yttria-stabilized zirconia (YSZ) layers. We investigated the dependences of crystallization on the Y content and cleaning solution for the YSZ layers. Transmission electron microscopy showed that some regions of the Si film deposited at 430 ^{o}C were directly crystallized on a YSZ layer without an amorphous region, where Si lattice fringes were tightly connected to YSZ lattice fringes. The crystallization of Si films on YSZ layers occurred at deposition temperatures lower than that on glass substrates by more than 100 ^{o}C. Zr, Y, and F concentrations in the Si film were negligible, except the Zr concentration near the interface. The discussion on the crystallization mechanism gave the following suggestions on the method of obtaining a high crystalline fraction. The YSZ layer should be chemically cleaned using a solution containing HF before Si film deposition, and the content ratio Y/(Zr+Y) of YSZ should be $\gtrsim$ 0.2.

1. Introduction

Poly- or microcrystalline silicon (poly-Si) films fabricated at low temperatures are of great interest for electron devices on temperature-sensitive and cheap substrates. A thin film transistor (TFT) in an active matrix flat panel display is one of the appropriate applications of the poly-Si films besides solar cells. Although hydrogenated amorphous silicon (a-Si:H) TFTs are currently used in commercialized displays, their low carrier mobility of less than 1 $cm^2/(V \cdot s)$ and their low reliability are the major drawbacks. Thus far, in order to obtain large grains with high carrier mobility, solid phase crystallization (SPC),[1-3] metal-induced crystallization (MIC),[4-7] metal-induced lateral crystallization (MILC),[8-11] and melting crystallization by pulse laser annealing (PLA)[12-14] have been proposed, in which a-Si films deposited on substrates are crystallized by annealing. The SPC method has the demerits of high process temperature (> 600 °C) and long annealing time (> 12 h). Although the MIC method overcomes these issues on the SPC method, it also has a serious problem of metal impurities, which are contained in crystallized films. The MILC method has been developed in order to overcome this problem, but the impurity concentration is still higher than $10^{18}/cm^3$.[11] The PLA method has advantages over the other methods, such as low thermal budget, large grain size, i.e., high mobility, and low impurity concentration. The equipment cost, however, is high, and a crystallized Si film has large roughness and random grain boundary location, which results in a low uniformity in device performance.[15] This is a problem, especially for large-size and current-drive displays.

Uniformity in device parameters, e.g., mobility and threshold voltage, or in the crystallinity of a poly-Si film over a large area is strongly required even though the grain size is less than 50 nm and the mobility is low [~5 $cm^2/(V \cdot s)$]. As a possible method of fabricating the desirable films, the direct deposition of poly-Si films has been investigated thus far by using various methods of chemical vapor deposition (CVD)[16-18] and sputtering,[19,20] in which

poly-Si films can be obtained at deposition temperatures lower than 500 °C. In general, poly-Si films deposited by these methods have columnar structures, and their grain sizes are less than 50 nm. Furthermore, a thin amorphous transition layer or an incubation layer is formed between the glass substrate and the polycrystalline region, and the crystallized films are much defective.[21-24] So, it has been reported often that the field effective mobilities of the films are as low as or lower those of a-Si TFTs.[24,25]

Alternatively, the use of an induction layer for low-temperature crystallization (crystallization-induction layer: CI layer) to cover an amorphous surface of a substrate has been proposed.[26-28] The CI layer, which is a polycrystalline dielectric, should have similar lattice constant and crystal structure to Si. The small lattice mismatch and same crystal structure give some advantages for low-temperature crystallization, although the heteroepitaxial growth of the Si film may not occur on the CI layer because of its too low process temperature. First, on the basis of the crystallographic information of the CI layer, the proposed method is considered to have the potential to reduce crystallization temperature, compared with conventional direct deposition methods. Second, on the basis of the crystallinity of the CI layer, it is possible to control the grain size and crystallographic orientation of a deposited Si film. Therefore, the CI layer method can be expected to produce poly-Si films at low temperatures in high mass production, and the films have a high uniformity in crystallinity as well as low impurity concentration and small surface roughness. It should be, however, noted that enlargement of grain size by this method is unpromising because of the direct deposition of the polycrystalline film.

As CI materials, ZrO_2[26] and CaF_2[27,28] have been proposed thus far. However, on the ZrO_2 layer, an amorphous incubation layer is formed, which means that ZrO_2 does not act as an actual CI material. CaF_2 is not an appropriate candidate material for electron devices owing to its low breakdown voltage and fluoride trap charges. On the other hand, our group

used a polycrystalline yttria-stabilized zirconia ($(ZrO_2)_{1-x}(Y_2O_3)_x$: YSZ) layer.[29] It has been reported that YSZ films can be grown heteroepitaxially at temperatures higher than 800 °C on Si and vice versa[30,31] because of the small lattice mismatch of ~ 5% with Si and the same cubic crystal structure. We have reported that Si films deposited on YSZ layers were crystallized, while Si films on glass substrates were still amorphous at the deposition temperature T_S = 430 °C.[32] It was also found that the chemical cleaning of the surface of a YSZ layer just prior to Si film deposition is a critical key process. After dipping YSZ layers into HF solution for removing contaminated and damaged surface layers, they were rinsed with ethanol solution or deionized water (DIW). The Si films deposited on the ethanol-rinsed YSZ layers were crystallized, but not those on the deionized-water (DIW)-rinsed YSZ layers. The following reason was proposed. During the HF etching process, F atoms adsorb on the YSZ layer surface. Even after the ethanol rinsing process, some of the F atoms remain on the layer surface, and the residual F atoms may protect the bare etched YSZ surface from exposure to contaminants in the preparation atmosphere. Just before Si film deposition in a vacuum chamber, most of the F atoms desorb at substrate heating. Therefore, the residual F atoms can contribute to the smooth transmission of crystallographic information from the YSZ surface to the deposited Si. Because the residual amount of F atoms after the DIW rinsing process was much smaller than that after the ethanol rinsing process, Si crystallization on the DIW-rinsed YSZ layers hardly occurred.

Recently, we have found that crystalline fractions of Si films were strongly dependent of the yttrium content ratios R_{YA} = Y/(Zr+Y) of as-deposited YSZ layers. R_{YA} in the previous report was less than 0.1.[32] However, when R_{YA} was 0.21, even on DIW-rinsed YSZ layers, the crystallization of Si films occurred at 430 °C.[33] In this paper, we show the inclusive investigation results of the Y content ratio dependence of Si film crystallization from R_{YA} = 0.02 to 0.3 as well as the rinse solution dependence, and discuss the crystallization

mechanism. Furthermore, we report on the distributions of the impurities Zr, Y, F, and O in the crystallized Si film and the deposition temperature dependence of Si crystalline fraction.

2. Experimental

The substrate was a 2×1 cm^2 fused quartz plate covered with a 70-nm-thick polycrystalline (111) YSZ layer, which was deposited by reactive magnetron sputtering with an Ar + O_2 mixture gas. The sputtering target was a Zr metal target, on which 8 pieces of 1×1 cm^2 Y were placed in a circular arrangement. The details were mentioned elsewhere.[34] Before the deposition of an Si film, the YSZ layer was dipped in a diluted 5% HF solution for 3 min to remove the contaminated and damaged surface layer. The HF-dipped YSZ layer was rinsed with ethanol solution or DIW just before being loaded into a deposition chamber. We deposited an a-Si film on the YSZ/quartz substrate by electron beam evaporation at a deposition temperature T_S of 300 to 550 °C with a deposition rate of 1 nm/min in ~10^{-6} Pa. The film thickness was mainly 60 nm, otherwise it will be mentioned. The crystallization fractions of the Si films were characterized by Raman spectroscopy using an excitation light of a 632.8 nm HeNe laser beam with a diameter of about 1 μm. The obtained Raman spectra were decomposed into the following three components: a crystalline component peak at 515−520 cm^{-1}, an amorphous component peak at around 480 cm^{-1}, and an intermediate component peak at 500 ~ 510 cm^{-1}, which is associated with bond dilation at grain boundaries. As an indication of crystalline fraction, we used a calculated value of the empirical expression $X_C = (I_c + I_m)/(I_c + I_m + \sigma I_a)$, where I_c, I_m, and I_a are the integrated intensities corresponding to the crystalline, intermediate, and amorphous component peaks, respectively, and σ is the ratio of the integrated Raman cross section for amorphous phase to crystalline phase. In this study, σ was chosen to be 1 for simplicity,[35-37] although it depends on the grain size and the energy of the excitation beam.[38,39] The microstructures of the Si

films were observed by transmission electron microscopy (TEM). The surface crystallinity of some samples was observed by *in situ* reflected high-energy electron diffraction (RHEED) during the Si film depositions. The chemical states of the YSZ surfaces were evaluated by X-ray photoelectron spectroscopy (XPS) using Al Kα (1486.6 eV) as an X-ray source and the take-off angle $\theta = 35°$. The binding energies (BEs) were calibrated using an adventitious carbon peak C 1*s* (284.6 eV) as a standard reference. In order to inhibit surface charging effects, a low-energy electron flood gun was used.[40,41] The Y content ratio of the YSZ layer was estimated from the integrated intensities of the Y 3*d* and Zr 3*d* peaks of XPS spectra, which were normalized by the atomic sensitivity factors. The estimation error was roughly determined to be $\pm$10 %. In this paper, we define yttrium ratio after chemical treatment as R_{YC}, since the chemical composition of the chemically treated YSZ surface was generally changed from that of the as-deposited YSZ surface, R_{YA}. Depth profiles of Zr, Y, F, and O in the deposited Si films were measured by secondary ion mass spectrometry (SIMS) in order to investigate the diffusion of impurities in 60 and 120-nm-thick Si films during the deposition.

3. Results

Figure 1 shows the Raman spectra of the Si films deposited on the YSZ layers and glass substrates, where (a) and (b) are for the ethanol-rinse and the DIW-rinse cases, respectively. The R_{YA} values for the ethanol-rinse case are 0.02 and 0.16, and those for the DIW-rinse case are 0.08 and 0.21. In each of the Si films on the glass substrates in both figures, we observe a broad and large peak around 480 cm^{-1} due to an a-Si phase. In Fig. 1(a) for the ethanol-rinse case, the spectra on the YSZ layers show sharp peaks at 518 cm^{-1} due to a crystalline silicon (c-Si) phase regardless of R_{YA}, where the intensity for the high $R_{YA} = 0.16$ is much larger than that for the low $R_{YA} = 0.02$. In Fig. 1(b) for the DIW-rinse case, however, the spectrum for the high $R_{YA} = 0.21$ shows a strong crystalline peak, and that for the low $R_{YA} = 0.08$ shows a

broad amorphous peak. The result in Fig. 1 suggests that both the types of rinse solution and Y content markedly influence the crystallization of the deposited Si films.

Figure 2 shows the dependence of Y content on the crystalline fraction X_C of the Si film. Squares and triangles indicate data for the ethanol-rinse and DIW-rinse cases, respectively. These symbols present the averages of 3 to 5 measurement points of one sample, and the top and bottom error bars indicate the maximum and minimum values, respectively. It can be seen that, in the low Y content region below R_{YA} = 0.10, the Si films on the ethanol-rinsed YSZ layers are crystallized, but those on the DIW-rinsed YSZ layers are fully amorphous. Furthermore, the X_C values for the ethanol-rinse case markedly fluctuate, which means that the degree of crystallization is not uniform on the entire YSZ layer even under the same deposition conditions of the Si films. Near R_{YA} = 0.10, the Si films deposited on the DIW-rinsed YSZ layers are crystallized slightly. The X_C values for both the ethanol- and DIW-rinse cases increase with Y content and become almost saturated around 50% when R_{YA} > 0.20. It can be concluded that, in the low Y content region, the ethanol rinsing process is more effective in inducing Si crystallization than the DIW rinsing process. The detailed mechanism will be discussed later.

The c-Si peak positions of the Raman spectra for the samples in Fig. 2 were independent of R_{YA} and within the range from 518 to 519 cm^{-1}, which is lower than 520 cm^{-1} for bulk c-Si. This means that the deposited Si films experience tensile stress.[42,43] The tensile stress of the deposited Si films is mainly caused by the difference between the thermal expansion coefficients of Si and glass, which are 2.8×10^{-6} and 0.5×10^{-6} /°C, respectively. The full-widths at half-maximum (FWHMs) of the peaks ranged from 6.5 to 7.5 cm^{-1}. These values were larger than 4.7 cm^{-1} for the measured bulk Si and 5.5 to 6.5 cm^{-1} for poly-Si films by PLA;[44] however, they were much smaller than the reported microcrystallite values of more than 10 cm^{-1}.[45] It has been reported that FWHM is strongly related to crystalline

defect density, i.e., a small FWHM for a small defect density.[44,46)] Therefore, this strong relationship indicates that the crystallized Si films produced by the CI method have higher defect densities than those produced by the PLA method; however, such defect densities are much smaller than those of microcrystallites.

We also monitored the *in situ* growth of the deposited Si film by RHEED. Figure 3 shows the (a) RHEED pattern of the bare YSZ layer at 430 °C and (b)−(d) those of the Si films deposited on the DIW-rinsed YSZ layers with R_{YA} = 0.13 at T_S = 430 °C in order of sequential deposition time. As a reference, a halo pattern of an amorphous Si (a-Si) film is also shown in Fig. 3(e). In Fig. 3(a), a spotty pattern is observed. Since the pattern from the YSZ layer was the same as that for any incident e-beam direction, it was found that the YSZ layer had a fiber texture or a preferential orientation of (111), which was in good agreement with the result of the XRD measurement. From the initial stage [Fig. 3(b)] to the final stage [Fig. 3(d)] of Si film deposition, the spot patterns can still be observed; however, they are more diffused than those in Fig. 3(a). From this result, it can be inferred that the crystallization of the Si film partially occurred on the DIW-rinsed YSZ layer during the deposition.

Figures 4(a) and 4(b), respectively, show the cross-sectional low-resolution and high-resolution (HR-) TEM images of the Si film deposited at T_S = 430 °C on the DIW-rinsed YSZ layer with R_{YA} = 0.21. The HR-TEM image in Fig. 3(b) shows a close-up image of one area around the interface, which is enclosed by a dotted frame in Fig. 4(a). This also shows the electron-diffraction (ED) patterns simulated by using the fast Fourier transform (FFT) based on the local lattice images enclosed by white and black square frames labeled as point 1 and point 2, respectively. Some large regions of the Si film grow directly from the YSZ layer without an amorphous transition region, although the other regions, e.g., point 3, are in the amorphous phase. For example, at the Si/YSZ interface of point 4, the start

points of the lattice fringe lines of the crystallized Si film coincide with the end points of the YSZ layer one by one. The strong spots in both the ED patterns correspond to {111} planes, except for the two spots of YSZ {200} indicated by white arrows. From these patterns, the crystallographic orientation normal to the interface can be identified as <111>, which is the preferential orientation of the YSZ layer. Both the ED patterns also show a {110} plane, although they are rotated by 180^{o} along the axis normal to the interface or <111>. This suggests that the crystallites of points 1 and 2 have a twinlike crystallographic relationship despite of heteromaterials. It has been well known that microtwins easily form in Si films grown epitaxially on Si(111) substrates[47-50] and in poly-Si films grwon by SPC.[51] It has also been reported that when the interface between the amorphous and crystalline phases is rough, microtwins are observed well often.[47] Thus, the twinlike relationship in our case may also be due to the roughness of the interface, as shown in Fig. 4. From this result, it can be considered that the nucleation was stimulated by the crystallographic information of the YSZ layer, from where the crystallization of the upper amorphous region occurred and progressed up to the surface. However, the crystallized Si regions contain many defects, e.g., twins and dislocations. The amorphous regions also exist in the Si film. We speculate the reason why mixture of amorphous and crystalline phases exists in the vicinity of the interface as follows: Just before the Si film deposition, the YSZ surface condition is not controlled perfectly and is not uniform over the entire area owing to grain boundaries, unremoved contaminants, microroughness, and so on. The X_C at R_{AY} = 0.2 in Fig. 2 is about 40%, which is small compared with that in the TEM images shown in Fig. 4, even though the errors in Raman measurement and its analysis are about 10%. The main reason for this is the assumption that the ratio of the integrated Raman cross section σ is set to be 1 for simple calculation. According to Bustarret et al.'s report,[38] σ can be expressed experimentally as $\sigma = 0.1 + \exp(-L/10)$ for a wavelength of 632.8 nm, where L is the grain size in nm. Using this equation,

the corrected crystalline fraction for X_C = 40% is calculated to be about 74% when the average grain size is L = 20 nm, taking the TEM images in Fig. 4 and the FWHM of the Raman spectra in Fig. 1 into account. This value seems to be reasonable for the TEM images.

Next, we observed XPS spectra from surfaces of YSZ layers. They can give us important information on the chemical bond states of the YSZ components from the viewpoint of the crystallization of the Si films deposited on the YSZ layers. Figure 5 shows the XPS spectra from the (i) as-deposited, (ii) HF-dipped, and (iii) DIW-rinsed YSZ layers with R_{YA} = 0.13. In this figure, two notable points are obsrved. One is the ratio of the yttrium Y 3*d* peak intensity to the zirconium Zr 3*d* peak intensity, and the other is the F 1*s* peak intensity due to F atoms adsorbed on the YSZ surface. The calculated Y content ratio of the HF-dipped YSZ layer was determined to be 0.33, which is much larger than the as-deposited YSZ layer R_{YA} = 0.13. However, after the DIW rising process, the Y content ratio becomes almost the same as the as-deposited YSZ layer value. In other words, both Y and Zr atoms are etched by HF dipping, but certain amounts of the etched and dissolved Y atoms adsorb on the YSZ layer surface. Most of them, however, are removed by DIW rinsing. The DIW rinsing process also removes the adsorbed F atoms, leaving a small amount of them. If Zr atoms are etched selectively by the HF solution and Y atoms are bonded to O atoms constructing the YSZ layer, the Y content ratio after the DIW rinsing process will be much higher than R_{YA} and will be near the value obtained after the HF dipping process.

Figure 6(a) shows the R_{YA} dependences of the Y content ratios of the chemically treated YSZ layers (R_{YC}), namely the HF-dipped layers without rinsing (circles), ethanol-rinsed layers (squares), and DIW-rinsed layers (triangles). It can be seen from this figure that the R_{YC} values of all the samples increase with R_{YA}. The R_{YC} values of the ethanol-rinsed layers are almost equal to those of the HF-dipped layers, and roughly twice larger than R_{YA}. The incremental Y ratio $\Delta R_{YC} = R_{YC} - R_{YA}$ is due to the adsorption of dissolved Y atoms in the

HF solution, as mentioned previously. In contrast, the R_{YC} of the DIW-rinsed YSZ layer is the lowest among the three treatments, being roughly proportional to R_{YA}, as indicated by the solid line $R_{YA} = R_{YC}$. However, for a high $R_{YA} \gtrsim 0.15$, R_{YC} has a slightly larger $\Delta R_{YC} \approx 0.05$ than R_{YA}. Figure 6(b) shows the relationship between R_{YA} and R_F, where R_F is the F ratio to Zr+Y, F/(Zr+Y), for the same chemically treated YSZ layers as those in Fig. 6(a). The R_F of any treated YSZ layer increases with R_{YA}, and the R_F of the DIW-rinsed layers is the lowest among the three treatments. The highest R_F is obtained from the as-HF-dipped layers, followed by that obtained from the ethanol-rinsed layers. It can be seen that 60−80% of the amount of adsorbed F atoms remains after the ethanol rinsing process, but only 25−35% of the amount of adsorbed F atoms remains after the DIW rinsing process. Furthermore, the R_F values for the two rinse solutions become saturated with increasing R_{YA} over 0.15. The saturation level of R_F for the ethanol-rinse case is ~1.0, which is twice that (~0.5) for the DIW-rinse case. Comparing Fig. 6(a) with Fig. 6(b), it seems that there is a relationship between the amounts of adsorbed Y and F atoms on the YSZ layers after the rising process. These phenomena will be discussed in detail later.

Figures 7(a) and 7(b) show the concentration depth profiles of Zr and Y, and O and F, respectively, in the 120-nm-thick Si film deposited on the ethanol-rinsed YSZ layer at 430 °C, where X_C was ~45% and R_{YA} was ~0.16. Figure 7(c) shows the concentration depth profiles of O and F in the 60-nm-thick Si film deposited on the DIW-rinsed YSZ layer at 430 °C. In this case, the Si film was amorphous because R_{YA} was low (~0.08), as shown in Fig. 2. Since the quantitative concentrations were estimated by using a standard sample of an ion-implanted amorphous Si, the concentrations in the Si film are valid in this figure. The concentrations near the interface and in the YSZ layer are incorrect because of the so-called matrix and charge-up effects due to the insulator of YSZ.[52] From Fig. 7(a), it can be seen that Zr atoms diffuse into the crystallized film slightly. The Zr concentration at the Si/YSZ

interface is about 5×10^{18} atoms/cm^3 and decreases towards the surface of the Si film below the background level of 2×10^{16} atoms/cm^3. It has been reported that Zr atoms from the ZrO_2 film hardly diffuse into Si even at 700 ^{o}C for 5 min for the application of a gate insulator.[53] In our case, a certain amount of chemically unstable Zr due to HF dipping might remain on the YSZ surface before the Si film deposition; however, a clear reason for this is not found at present. Unlike Zr, the Y signal is below the background level, thus, Y can be a negligible impurity in the Si film. Although the Zr and Y concentrations for the DIW-rinse case are not shown here, they are considered to be the same as those in Fig. 7(a) because there is no essential difference between the two processes with respect to diffusion. From this result, we can consider that the diffusion of Zr and Y into the deposited Si film from the YSZ layer is negligible, except in the vicinity of the interface. We should further suppress the diffusion of Zr near the interface for device application.

In Fig. 7(b), it can be seen that the O and F concentrations for the ethanol-rinse case are on the orders of 1×10^{18} and 1×10^{17} atoms/cm^3, respectively, in the bulk of the Si film. Although the O concentration is negligible for device performance, the F concentration seems relatively higher. In contrast, in Fig. 7(c) for the DIW-rinse case, the F concentration is less than 1×10^{16} atoms/cm^3 in the bulk of the Si film and much smaller than that in Fig. 7(b). This concentration as well as the O concentration is acceptable for obtaining a high device quality. The two reasons for the lower F concentration for the DIW-rinse case can be considered to be 1) the higher rinsing effect for removing the residual adsorbed F atoms and 2) the evaporation of F atoms from the YSZ layer by heating at T_S = 430 ^{o}C in the vacuum chamber. For the ethanol-rinse case, a certain amount of adsorbed F atoms remains even after substrate heating, as indicated in the previous report.[32] In both Figs. 7(b) and 7(c), the O and F concentrations increase toward the surface of the Si film. Probably, O atoms adsorbed on the Si film from the atmosphere and then diffused into the film. F atoms also probably

adsorbed on the Si film chemically cleaned by using the HF solution to remove the native oxide before the SIMS measurement. However, even after the DIW rinsing process, a small amount of adsorbed F atoms might remain on the Si film.

The deposition temperature T_S dependences of the crystalline fractions X_C for the ethanol-rinse cases are shown in Fig. 8. Closed squares and open squares indicate the data for the Si films deposited on the YSZ layers with $R_{YA} \gtrsim 0.13$ and on the glass substrates without a YSZ layer, respectively. It can be seen that, at $T_S < 400$ °C, the Si films deposited on the glass substrates are fully amorphous, but those on the YSZ layers are partially crystallized. By increasing the T_S to 430 °C, the Si film on the glass substrate starts crystallizing. The X_C values of both films increase with T_S and tend to saturate at ~60% at temperatures above 500 °C. From this result, it can be considered that the nucleation rate of Si is strongly dependent of the interface material, but the saturation level of X_C is almost independent of it. Actually, at $T_S > 500$ °C, the CI layer effect of YSZ may become negligible. This is probably because a higher T_S or a higher thermal energy enhances more the surface migration of the deposited Si; thus, the Si film is crystallized without the effect of the interface material. Therefore, it is supposed that, above $T_S = 500$ °C, the same crystalline quality of the initial Si layers on the YSZ layer and glass substrate leads to the same crystalline fraction of X_C, as shown in Fig. 8. Although the T_S dependence of X_C has not been investigated for the DIW-rinsed YSZ layer, the tendency will almost be the same as that in Fig. 8, provided that $R_{YA} \gtrsim 0.2$.

Figures 9(a)−9(c) show the surfaces of the Si films deposited at $T_S = 320$, 350, and 430 °C, respectively, on the ethanol-rinsed YSZ layers, which were observed by SEM. The Si films were Secco-etched to delineate grain boundaries before the observation. The arrow in Fig. 9(c) indicates a hole formed by Secco-etching a local amorphous region. The X_C values for $T_S = 320$, 350, and 430 °C are 1.5, 18, and 37%, respectively. In this figure, the crystallized grains are observed on the etched Si film deposited even at 320 °C. This means

that the critical deposition temperature for crystallization on the YSZ layer is as low as 320 °C, which is in good agreement with that in Fig. 8. It can also be seen that the Si grain density increases with T_S, although the uniformity of grain size is reduced with it. This is probably because the nucleation rate increases with T_S. According to the result in Fig. 4, it can be inferred that the nucleation sites locate on the YSZ layer, and that the growth front proceeds not only upward in height but also laterally in width during the deposition. When the deposition temperature is 320 °C, the nucleation density on the YSZ layer is so low that the distance between the nucleation sites (DN) may be larger than the final size of the grain. Therefore, since the grains can be grown without collision with one another up to the final deposition thickness, they are similar in size. When the deposition temperature is set higher, e.g., T_S = 430 °C, the nucleation density increases such that some lateral growth fronts of grains may impinge with one another randomly during the deposition. As a result, the distribution of grain size becomes nonuniform compared with those in the lower T_S cases as shown in Fig. 9(c). In the future, we should investigate the relationship between the YSZ and crystallized Si grains in terms of size and orientation.

4. Discussion

In this section, we discuss the crystallization mechanism of the Si films deposited on the chemically treated YSZ layers at the low temperature of 430 °C. Under this condition, the Si films deposited directly on the glass substrates are amorphous. Particularly, we focus on the dependence of the crystalline fraction on the as-deposited Y content ratio R_{YA}, as shown in Fig. 2. From Figs. 2 and 6(b), it can be seen that, for the DIW-rinse case, when R_{YA} decreases from 0.15 to less than 0.08, the crystalline fractions X_C markedly decrease from about 30% to zero, although the F ratios R_F decrease slightly. On the other hand, as mentioned in the previous report,[34] R_{YA} affects the crystal structure and crystalline quality of

YSZ layers. At a very low $R_{YA} \leq 0.02$, YSZ films are in monoclinic phase with a low crystalline quality. As R_{YA} increases, crystal structures transform to a more stable tetragonal phase with a higher crystalline quality, followed by a cubic phase. From these results, it is supposed that important factors for the low-temperature crystallization of Si films are not only surface protection due to F atoms adsorbed on the YSZ layers but also the YSZ surface crystalline quality.

Figure 10(a) shows the two narrow scan XPS spectra of Zr 3*d* from the DIW-rinsed YSZ layers with the high $R_{YA} = 0.21$ and low $R_{YA} = 0.07$, compared with the spectrum from the as-deposited YSZ layer with the high $R_{YA} = 0.21$. The RHEED pattern is also shown, which is mentioned later. The shapes of the Zr 3*d* peaks from both the DIW-rinsed YSZ layers are similar to that from the as-deposited YSZ layer. The shape of the Zr 3*d* peak from the HF-dipped YSZ layer, not shown here, is also almost the same as that from the as-deposited YSZ layre. These results mean that the chemical state of surface Zr within the escape depth of ~2 nm[55] is hardly changed by the cleaning processes. However, the peak of the low R_{YA} is shifted to an energy higher than that of the high R_{YA} by ~ 0.5 eV because of a chemical shift caused by increasing yttrium content.[55] Figure 10(b) shows the three narrow-scan XPS spectra of Y 3*d* from the DIW-rinsed YSZ layers with the high $R_{YA} = 0.21$ and low $R_{YA} = 0.07$, and from the ethanol-rinsed YSZ layer with the low $R_{YA} = 0.06$. As a reference, the spectrum from the as-deposited YSZ layer with the high $R_{YA} = 0.21$ is also shown. The Y 3*d* signals are split into the two peaks or doublets, $3d_{5/2}$ and $3d_{3/2}$, due to spin-orbit coupling, which holds true for Zr 3*d*, as shown in Fig. 10(a). The arrows in the figure indicate the literature values of binding energies (BEs) of Y_2O_3,[54,55] yttrium-bonded with a hydroxide Y-OH,[55] and YF_3.[54,56,57] It can be seen in this figure that the shape from the DIW-rinsed YSZ layer with the high $R_{YA} = 0.21$ is similar to that from the as-deposited YSZ layer. However, the shapes of the other two spectra from the low $R_{YA} = 0.07$ and 0.06 are much different from them and

apparently broader. The spectrum from the DIW-rinsed YSZ layer with the low R_{YA} = 0.07 has some high-BE subcomponents, such as Y-OH and YF_3, as well as a main component, which is Y_2O_3. The spectrum from the ethanol-rinsed YSZ layer with the low R_{YA} = 0.06 also shows the same subcomponents. In this case, particularly, the YF_3 component at around 160 eV is very strong, as reported previously.[32] Furthermore, it seems that the two spectra from the DIW-rinsed layers also overlap slightly with small signals due to YF_3. The result indicating that F ions preferentially bond to Y ions over Zr ions coincides with the following reports. When YSZ is dipped into HF solution, Zr is solved as an anionic fluoride complex ion, such as $[ZrF_6]^{2-}$.[58] As for Y, it has been reported that, although Y is also solved, insoluble YF_3 is formed on the surface of YSZ in the HF solution.[59] Thus, we observe Y bonded to F in the XPS spectra of YF_3.

It was observed that the shape of Y 3*d* from the HF-dipped YSZ layer was similar to that from the ethanol-rinsed YSZ layer. According to this result and the result shown in Fig. 6(a), where the R_{YC} of the ethanol-rinsed layer is almost equal to that of the HF-dipped YSZ layer, it can be considered that Y atoms bonded to F atoms are hardly removed by ethanol rinsing. However, as shown in Fig. 6(b), a certain amount of F atoms adsorbed on the HF-dipped YSZ layer is removed by ethanol rinsing. The removed F may be bonded to other positive ions, except Y ions. Therefore, it can be considered that ethanol rinsing process hardly removes YF_3 molecules adsorbed on the HF-dipped YSZ layer. Furthermore, the DIW rinsing process can wash away more F atoms as well as Y atoms bonded to F, but not completely. This is probably because the dielectric constant ε of water (~78) at room temperature (RT) is much higher than ~25 for ethanol at RT. The higher ε reduces the ionic bond strength due to Coulomb force. Thus, the ethanol rinsing process can hardly wash away F atoms bonded to Y atoms, but it can remove F atoms bonded weakly to other ions. In contrast, the DIW rising process can easily remove F atoms bonded to Y atoms. However, the removal of F atoms is

partial and a certain amount of F atoms still remains on the YSZ layer, as shown in Fig. 6(b). Owing to a slightly higher shoulder peak intensity at around 159 eV in Fig. 10(b), it is supposed that the remaining F atoms are partially bonded to Y atoms even after the DIW rinsing process.

On the other hand, Fig. 10 also shows the RHEED pattern of the DIW-rinsed YSZ layer with the low R_{YA} = 0.07 at 430 °C just before the Si film deposition. This pattern is more diffused than the pattern of the high R_{YA} [Fig. 3(a)]. This indicates that the surface crystalline quality with the low R_{YA} is lower than that with the high R_{YA}. According to the XPS spectra and RHEED pattern in Fig. 10, we can speculate as follows: The low quality YSZ surface with the low R_{YA} may be much chemically active. If there is no sufficient amount of F atoms to cover the entire YSZ surface, which may occur at a small R_F, the chemically active sites may enhance the direct adsorption of contaminants on the YSZ layer from the experimental environment. As well known,[60-62] the contaminants are probably hydrocarbon, oxidized carbon and/or oxidized hydrocarbon adsorbed on the chemically treated surface. These contaminants are not only from the laboratory room but also from the vacuum chamber. In fact, signals due to C were inevitably observed in the XPS spectra from the YSZ layers in our work.

On the basis of the above-mentioned experimental results and discussion, we consider a comprehensive mechanism for the Si film crystallization using the schematic diagrams in Fig. 11. The surface of the as-deposited YSZ layer is damaged by highly energetic particle bombardment during sputtering deposition and contaminated by exposure to the atmosphere. The damaged and contaminated layer is removed or etched by HF dipping, which provides crystallographic ordered sites at the surface. Simultaneously, a large amount of F atoms, as well as etched and dissolved Y atoms, are adsorbed on the surface. Furthermore, as mentioned in Fig. 6, the amounts of adsorbed Y (R_{YC}) and F (R_F) atoms increase with R_{YA}

owing to the HF dipping process. After the ethanol rinsing process, F atoms bonded to Y atoms remain as YF_3 molecules on the YSZ surface and some F atoms without Y are removed since the R_{YC} and XPS spectrum of Y are almost the same as those of the HF-dipped YSZ layer. On the other hand, although the DIW rinsing process removes larger amounts of adsorbed F and Y atoms, certain amounts of absorbed F and Y atoms still remain on the YSZ layer. In particular, for a high $R_{YA} \gtrsim 0.15$ ($\Delta R_{YC} \approx 0.05$), R_F becomes saturated at ~0.5.

Because the saturation of R_F is an important phenomenon for the low-temperature crystallization of the Si film, we discuss it in more detail using a model as follows: It is speculated that, after the DIW rinsing process, the surface of the YSZ layer with $R_{YA} \gtrsim 0.2$ is covered almost fully with one monolayer consisting of F+Y ions. The excess F+Y ions over one monolayer, which are generated by HF dipping, are removed by DIW rinsing. The ethanol rinsing process may leave about two F+Y monolayers since R_F after the ethanol rinsing process is about twice that after the DIW rinsing process, as shown in Fig. 6(b). The lower and upper monolayers on the ethanol-rinsed YSZ layer might be bound through Coulomb attractive interaction among the constructing ions. However, this interaction is not so strong that the upper layer can be removed by rinsing with DIW whose dielectric constant is much larger than the ethanol one. Some F ions in the F+Y monolayer on the DIW-rinsed YSZ layer are bonded to Y ions constructing the surface of the YSZ layer. Since one of the three bonds of Y^{3+} ion must be bound to one O^{2-} ion in the YSZ layer, the other two bonds are bound to the two F^- ions in the monolayer. This is similar to O-Y-F_2. On the other hand, Y^{3+} ions in the monolayer, which corresponds to $\Delta R_{YC} \approx 0.05$, are bound to three F^- ions to form YF_3. Since the Coulomb interaction between the F+Y monolayer and the YSZ layer may be strong, the DIW rinsing process is supposed to hardly remove the monolayer.

Using the above-mentioned model, we estimate the area densities of Y^{3+} ions bonded with three F^- ions in the monolayer, σ_{Ym}, and Y^{3+} ions bonded with two F^- ions and one O^{2-}

ion, σ_{YY}. The area density of total F^- ions is defined as $\sigma_F = 3\sigma_{Ym} + 2\sigma_{YY}$. Using $R_{YC} \approx 0.25$ at $R_{YA} \approx 0.2$, take-off angle $\theta = 35°$, YSZ lattice constant $a = 0.514$ nm,[63] F^- ion radius $r_F = 0.133$ nm,[64] and the escape depth of Zr 3*d* and Y 3*d* photoelectrons $\lambda = 2$ nm,[55] we can calculate $\sigma_{mY} = 1.95$ nm^{-2}, $\sigma_{YY} = 3.03$ nm^{-2}, and $\sigma_F = 11.91$ nm^{-2}. The detailed derivations are mentioned in Appendix. If the F^- and Y^{3+} ions have the same effective radius r_e and construct one closely packed F+Y monolayer, r_e can be calculated to be 0.144 nm. This radius is near the literature radius $r_F = 0.133$ nm and is not very far from the literature radius of Y^{3+} (0.102 nm).[64] Considering the Coulomb repulsion of negative F^- ions one another in the monolayer, the calculated r_e value seems to be reasonable. Furthermore, since R_F can be expressed as

$$R_F = \frac{\sigma_F}{\rho\lambda' \sin\theta + \sigma_{mY}} \quad . \qquad (1)$$

ρ is the atomic volume density of Zr + Y in YSZ and $\lambda' = \lambda - 2r_F$, where λ' is an effective escape depth of λ subtracted by one F^- ion size in the case of one monolayer on the DIW-rinsed YSZ layer. From eq. (1), we obtain an R_F of about 0.38, using the above estimated values of σ_F and σ_{mY}. This R_F value is not far from the experimental saturation value of ~0.5. Their difference may be ascribed to the used assumptions. With respect to bonding, for example, a hydrogen bond is formed to connect two F ions, the number of F ions attracted by Y^{3+} ions (i.e., coordination number) would be more than 2 for σ_{YY} or/and 3 for σ_{mY}, and so on. Furthermore, there is a possibility that the used λ' value would be not well approximated. Thus, it can be said that the model of one F+Y monolayer formation is roughly valid. That is, F and Y ions in the monolayer would be so arranged that the layer packing density is be maximized. When R_{YA} is nearly more than 0.2, the highest density may be achieved and no more F and Y ions could get into the layer.

During sample preparation and transportation prior to Si film deposition, contaminants

from the laboratory atmosphere adsorb on the surface of the chemically cleaned YSZ layer. At $R_{YA} \gtrsim 0.15$, R_F is more than ~0.45, such that the chemically adsorbed F covers the YSZ surface almost fully, as mentioned above. Thus, the F+Y monolayer acts as a layer that protects the clean YSZ surface from the contaminants. However, when R_{YA} is lower than ~0.07, R_F is less than 0.4 for not only the DIW-rinsed YSZ layer but also the ethanol-rinsed YSZ layer. Under this condition, some local areas with an insufficient coverage of the F+Y monolayer on the YSZ surface possibly allow the direct contact of contaminants from the environment. Furthermore, the low quality of the YSZ surface with the low R_{YA} may induce a higher level of adsorption of contaminants. Particularly, on the surface of the DIW-rinsed YSZ layer, water H_2O and hydroxides –OH may adsorb, as shown in Fig. 10(b).

When the substrate is heated up to the deposition temperature in the vacuum chamber just before Si deposition, most of the residual adsorbed F atoms evaporate, while the excess Y atoms remain, as mentioned in the previous report.[32] At the same time, most of the contaminants adsorbed on the F+Y monolayer may also evaporate; some of them chemically react with F. When $R_{YA} \gtrsim 0.15$, the clean surface of the YSZ layer appears with the crystallographically ordered sites. Therefore, the crystallographic information regarding the YSZ layer can result in the crystallization of the deposited Si film, which may be easier for arriving Si atoms to nucleate even at low deposition temperatures, and we can obtain Si films with high crystalline fractions on the YSZ layers with high R_{YA} values for both ethanol- and DIW-rinse cases. On the other hand, for a low $R_{YA} < 0.07$, although the residual adsorbed F atoms are evaporated by heating the sample, the surface of the YSZ layer is not as clean and pure as the higher R_{YA} layer. Since R_F is smaller than 0.4, in particular, for the DIW-rinse case, some areas of the YSZ surface directly react with the adsorbed contaminants; thus, they may be modified into other phases and disordered. This reaction and modification may be enhanced by the low crystalline quality of the YSZ surface with the low R_{YA}. The chemical

modification disturbs the transmission of the crystallographic information regarding the YSZ surface to the arriving Si atoms. As a result, on the YSZ layers with the lower R_{YA}, Si nucleation and the subsequent crystallization of Si films hardly occur. However, in the local areas of the ethanol-rinsed YSZ layer, Si crystallization occurs, as shown in Figs. 1 and 2. This is because F+Y monolayer islands are formed in the local areas of the YSZ surface; thus, they can protect the bare surface from contaminants locally. The entire YSZ surface is partially covered with the monolayer islands. The formation of the monolayer islands can be observed in Fig. 6, where, for the ethanol-rinse case at around $R_{YA} = 0.06$, R_{YC} is obviously larger than R_{YA} and R_F is around 0.3. At $0.1 \leq R_{YA} < 0.15$, since the coverage of one F+Y monolayer on the DIW-rinsed YSZ layer is partial, X_C is also in transition from zero to the saturated value.

As mentioned above, this mode can explain the experimental results qualitatively. However, it is not sufficient and is not beyond speculation since we do not have any clear evidence for the existence of contaminated areas at the interface under the amorphous Si regions yet. Thus, we should further investigate the interface properties in more detail.

5. Conclusions

We investigated comprehensively the Y content and rinse solution dependences of the crystallization of Si films deposited on glass substrates covered with poly-(111)YSZ layers at deposition temperatures T_S lower than 550 ^oC. From the cross-sectional HR-TEM image of the Si film deposited at 430 ^oC, it was found that some regions were crystallized directly on the YSZ layer without an amorphous transition layer, where Si lattice fringes were tightly connected to YSZ lattice fringes. Furthermore, it was found that the crystallization of the deposited Si films occurred on YSZ layers at T_S lower than that on glass substrates without YSZ layers by more than 100 ^oC. Therefore, it can be concluded that the poly-YSZ layer

induces and stimulates the crystallization of the deposited Si film at lower temperatures, compared with the case of direct deposition on glass substrates. The impurity concentrations of Y and F, which diffused from the YSZ layers into the Si films, were negligible and less than 2×10^{16} and 1×10^{16} atoms/cm^3, respectively. The Zr concentration in the film bulk was ~1×10^{16} atoms/cm^3, but that near the interface was relatively high, i.e., ~5×10^{18} atoms/cm^3.

From the above-mentioned results, the crystallization mechanism was discussed. The discussion leads to the next important suggestions on the method of obtaining a high crystalline fraction of the Si film. 1) Prior to Si film deposition, the YSZ layer should be chemically cleaned with a solution containing HF. By this treatment, the damaged and disordered surface layer is removed, and then the surface is covered with adsorbed F atoms. 2) The Y content ratio of YSZ, R_{YA}, should be roughly more than 0.2. The amount of adsorbed F atoms on the YSZ surface increases with R_{YA} and saturates at $R_{YA} \gtrsim 0.15$. Thus, $R_{YA} \gtrsim 0.2$ may guarantee that one F+Y monolayer covers the clean YSZ layer fully, which is sufficient for protecting the YSZ surface from contaminants in the atmosphere. Furthermore, the crystalline quality and stability of the YSZ layer with $R_{YA} \gtrsim 0.2$ are superior to those of the layer with a low $R_{YA} < 0.07$. Therefore, it can be speculated that, at $R_{YA} \gtrsim 0.2$, the crystallographic information regarding the YSZ layers is smoothly transmitted to the deposited Si films; thus, so that Si crystallization might be induced at lower temperatures.

From this study, it can be considered that the CI layer method is a useful direct deposition technique for obtaining a crystallized Si film with a uniform crystalline quality and no incubation layer at low temperatures in the entire deposition area. However, from now on, we should work on reducing the Zr concentration for device performance and on investigating the crystallographic relationship of each grain between the poly-YSZ layer and the crystallized Si film on it.

Acknowledgement

This work was partially supported by a Grant-in-Aid for Scientific Research C (No. 21560324) from the Japan Society for the Promotion of Science.

Appendix

Because YSZ is a CaF_2 crystal structure, ρ is $4/a^3$. Using ρ and the atomic volume density of Y (ρ_Y), R_{YA} and R_{YC} can be expressed as

$$R_{YA} = \frac{\rho_Y}{\rho}, \qquad \text{(A·1)}$$

$$R_{YC} = \frac{\rho_Y \lambda' \sin\theta + \sigma_{mY}}{\rho\lambda' \sin\theta + \sigma_{mY}}, \qquad \text{(A·2)}$$

considering one F+Y monolayer on a DIW-rinsed YSZ layer. $\rho\lambda'\sin\theta$ is the area atomic Zr+Y density of the YSZ layer under the monolayer in the measurement of XPS at $\theta = 35^o$.

Using eqs. (A·1) and (A·2), we obtain

$$\sigma_{mY} = \rho\lambda' \sin\theta \frac{(R_{YC} - R_{YA})}{(1 - R_{YC})}. \qquad \text{(A·3)}$$

Next, we consider the number of Y^{3+} ions of the YSZ layer, which attract F^- ions in the monolayer. It is assumed that the Y ions originate from the first and second Zr+Y atomic layers of a cubic (100) YSZ on average. From this assumption, σ_{YY} is equal to $a\rho_Y = a\rho R_{YA}$; thus, σ_F can be expressed as

$$\sigma_F = 3\sigma_{mY} + 2\sigma_{YY} = 3\sigma_{mY} + 2a\rho R_{YA}. \qquad \text{(A·4)}$$

Per unit cell area of a^2 at $R_{YA} = 0.2$, we can estimate the average numbers of Y in one monolayer and Y attracting F ions in the YSZ layer. That is, $a^2\sigma_{mY} \approx 0.52$ and $a^2\sigma_{YY} = a^3\rho R_{YA} \approx 0.80$. Thus, the number of F ions per a^2 in one monolayer can be calculated as $a^2\sigma_F \approx 3.2$.

On the other hand, if the F^- and Y^{3+} ions have the same effective radius r_e and construct one close-packed F+Y monolayer, $\sigma_F + \sigma_{mY}$ can also be expressed with r_e as

$$\sigma_F + \sigma_{mY} = \frac{1}{2\sqrt{3}r_e^{\,2}}. \qquad \text{(A·5)}$$

1) C. Ipri and G. Kaganowicz: IEEE Trans. Electron Devices **35** (1988) 708.
2) K. Nakazawa and K. Tanaka: J. Appl. Phys. **68** (1990) 1029.
3) L. Haji, P. Joubert, J. Stoemenos, and M. A. Economou: J. Appl. Phys. **75** (1994) 3944.
4) S. F. Gong, H. T. G. Hentzell, A. E. Robertsson, L. Hultman, S.-E. Hörnström, and G. Radnoczi: J. Appl. Phys. **62** (1987) 3726.
5) S. Y. Yoon, K. H. Kim, C. O. Kim, J. Y. Oh, and J. Jang: J. Appl. Phys. **82** (1997) 5865.
6) S. Y. Yoon, S. K. Kim, J. Y. Oh, Y. J. Choi, W. S. Shon, C. O. Kim, and J. Jang: Jpn. J. Appl. Phys. **37** (1998) 7193.
7) J.-Y. Kim, J.-W. Han, J.-M. Han, Y.-H. Kim, B.-Y. Oh, B.-Y. Kim, S.-K. Lee, and D.-S. Seo: Appl. Phys. Lett. **92** (2008) 143501.
8) S.-W. Lee, Y.-C. Jeon, and S.-K. Joo: Appl. Phys. Lett. **66** (1995) 1671.
9) S.-I. Jun, Y.-H. Yang, J.-B. Lee, and D.-K. Choi: Appl. Phys. Lett. **75** (1999) 2235.
10) C.-Y. Hou and Y. S. Wu: Jpn. J. Appl. Phys. **44** (2005) 7327.
11) M. Wong, Z. Jin, G. A. Bhat, P. C. Wong, and H. S. Kwok: IEEE Trans. Electron Devices **47** (2000) 1061.
12) T. Sameshima, S. Usui, and M. Sekiya: IEEE Electron Device Lett. **7** (1986) 276.
13) K. Sera, F. Okumura, H. Uchida, S. Itoh, S. Kaneko, and K. Hotta: IEEE Trans. Electron Devices **36** (1989) 2868.
14) J.-M. Shieh, Z. H. Chen, B.-T. Dai, Y.-C. Wang, A. Zaitsev, and C.-L. Pan: Appl. Phys. Lett. **85** (2004) 1232.
15) M.-K. Han, S.-G. Park, and H.-S. Shin: Proc. 15th Int. Display Workshops (IDW'08), 2008, p. 585.
16) T. Nagahara, K. Fujimoto, N. Kohno, Y. Kashiwagi, and H. Kakinoki: Jpn. J. Appl. Phys. **31** (1992) 4555.
17) S. Ishihara, D. He, M. Nakata, and I. Shimizu: Jpn. J. Appl. Phys. **32** (1993) 1539.

18) H. J. Lim, B. Y. Ryu, and J. Jang: Appl. Phys. Lett. **66** (1995) 2888.
19) Y. Mishima, M. Takei, T. Uematsu, N. Matsumoto, T. Kakehi, U. Wakino, and M. Okabe: J. Appl. Phys. **78** (1995) 217.
20) J. Joo: J. Vac. Sci. Technol. A **18** (2000) 2006.
21) M. Luysberg, P. Hapke, R. Carius, and F. Finger: Philos. Mag. A **75** (1997) 31.
22) H. Fujiwara, M. Kondo, and A. Matsuda: Phys. Rev. B **63** (2001) 115306.
23) J. Bailat, E. V.-Sauvain, L. Feitknecht, C. Droz, and A. Shah: J. Appl. Phys. **93** (2003) 5727.
24) A. J. Flewitt and W. I. Milne: in *Thin Film Transistors Materials and Processes*, ed. Y. Kuo (Kluwer Academic Publishers, Dordrecht, 2004) Vol. 1, p. 33.
25) M. W. D. Froggatt, W. I. Milne, and M. J. Powell: Mater. Res. Soc. Symp. Proc. **467** (1997) 893.
26) C. W. Han, J. H. Park, S. M. Han, M. K. Han, K. Y. Kim, I. J. Chung, S. J. Yun, and J. W. Lim: Jpn. J. Appl. Phys. **45** (2006) 4366.
27) D. Y. Kim, B. J. Ahn, S. I. Moon, C. Y. Won, and J. Yi: Sol. Energy Mater. Sol. Cells **70** (2002) 415.
28) J. K. Ko, D. Y. Kim, J. H. Park, S. W. Choi, S. H. Park, and J. Yi: Thin Solid Films **427** (2003) 259.
29) S. Horita, K. Kanazawa, K. Nishioka, K. Higashimine, and M. Koyano: Mater. Res. Soc. Symp. Proc. **910** (2006) 0910-A21-17.
30) I. Golecki, H. M. Manasevit, L. A. Moudy, J. J. Yang, and J. E. Mee: Appl. Phys. Lett. **42** (1983) 501.
31) S. Horita, M. Muranaka, and T. Fujiyama: Jpn. J. Appl. Phys. **34** (1995) 1942.
32) S. Horita and H. Sukreen: Appl. Phys. Express **2** (2009) 041201.
33) S. Hana , T. Akahori, and S. Horita: Proc. 16th Int. Display Workshops (IDW'09), 2009,

p. 271.
34) S. Hana and S. Horita: Thin Solid Films **517** (2009) 5830.
35) M. Wakagi, T. Kaneko, K. Ogata, and A. Nakano: Mater. Res. Soc. Symp. Proc. **283** (1993) 555.
36) T. Kaneko, M. Wakagi, K. Onisawa, and T. Minemura: Appl. Phys. Lett. **64** (1994) 1865.
37) E. A. T. Dirani, A. M. Andrade, L. K. Noda, F. J. Fonseca, and P. S. Santos: J. Non-Cryst. Solids **273** (2000) 307.
38) E. Bustarret, M. A. Hachicha, and M. Brunel: Appl. Phys. Lett. **52** (1988) 1675.
39) D. Han, G. Yue, J. D. Lorentzen, J. Lin, H. Habuchi, and Q. Wang: J. Appl. Phys. **87** (2000) 1882.
40) W. M. Lau: J. Appl. Phys. **67** (1990) 1504.
41) T. L. Barr: *Modern ESCA: The Principles and Practice of X-ray Photoelectron Spectroscopy* (CRC Press, Boca Raton, FL, 1994) Chap. 7, p. 133.
42) K. Kitahara, A. Moritani, A. Hara, and M. Okabe: Jpn. J. Appl. Phys. **38** (1999) L1312.
43) P. Lengsfeld, N. H. Nickel, Ch. Genzel, and W. Fuhs: J. Appl. Phys. **91** (2002) 9128.
44) K. Kitahara, R. Yamazaki, T. Kurosawa, K. Nakajima, and A. Moritani: Jpn. J. Appl. Phys. **41** (2002) 5055.
45) Z. Iqbal, S. Vepřek, A. P. Webb, and P. Capezzuto: Solid State Commun. **37** (1981) 993.
46) H. Richter, Z. P. Wang, and L. Ley: Solid State Commun. **39** (1981) 625.
47) R. Drosd and J. Washburn: J. Appl. Phys. **53** (1982) 397.
48) J. T. McGinn, L. Jastrzebski, and J. F. Corboy: J. Electrochem. Soc. **131** (1984) 398.
49) H. Yamamoto, H. Ishiwara, and S. Furukawa: Jpn. J. Appl. Phys. **24** (1985) 411.
50) C. I. Drowley, G. A. Reid, and R. Hull: Appl. Phys. Lett. **52** (1988) 546.
51) A. Nakamura, F. Emoto, E. Fujii, Y. Uemoto, A. Yamamoto, K. Senda, and G. Kano: Jpn. J. Appl. Phys. **27** (1988) L2408.

52) R. G. Wilson, F. A. Stevie, and C. W. Magee: *Secondary Ion Mass Spectroscop*y (Wiley, New York, 1989) Chap. 2.3.
53) W.-J. Qi, R. Nieh, B. H. Lee, L. Kang, Y. Jeon, K. Onishi, T. Ngai, S. Banerjee, and J. C. Lee: IEDM Tech. Dig., 1999, p. 145.
54) *Handbook of X-ray Photoelectron Spectroscopy*, ed. C. D. Wagner, W. M. Riggs, L. E. Davis, J. F. Moulder, and G. E. Muilenberg (Perkin-Elmer, Eden Prairie, MN, 1979).
55) D. Majumdar and D. Chatterjee: J. Appl. Phys. **70** (1991) 988.
56) N. Y. Kirikova, J. C. Krupa, V. N. Makhov, and C. Severac: J. Electron Spectrosc. Relat. Phenom. **122** (2002) 85.
57) G. G. Condorelli, G. Anastasi, and I. L. Fragalà: Chem. Vapor Deposition **11** (2005) 324.
58) S. Balasubramanian and S. Raghavan: Jpn. J. Appl. Phys. **47** (2008) 4502.
59) F. Shojai and T. A. Mäntylä: Ceram. Int. **27** (2001) 299.
60) T. Takahagi, I. Nagai, A. Ishitani, and H. Kuroda: J. Appl. Phys. **64** (1988) 3516.
61) S. R. Kasi, M. Liehr, P. A. Thiry, H. Dallaporta, and M. Offenberg: Appl. Phys. Lett. **59** (1991) 108.
62) P. J. Talyor, W. A. Jesser, M. Martinka, K. M. Singley, J. H. Dinan, R. T. Lareau, M. C. Wood, and W. W. Clark III: J. Vac. Sci. Technol. A **17** (1999) 1153.
63) H. G. Scott: J. Mater. Sci. **10** (1975) 1527.
64) H. T. Evans, Jr.: in *Handbook of Chemistry and Physics*, ed. D. R. Lide (CRC Press, Boca Raton, FL, 1993) 74th ed., p. 12-8.

Figure captions

Fig. 1. (Color online) Raman spectra of the Si films deposited on the (a) ethanol-rinsed and (b) DIW-rinsed YSZ layers. For comparison, (a) and (b) show the spectra from the Si films deposited on the ethanol-rinsed and DIW-rinsed glass substrates, respectively.

Fig. 2. (Color online) Y content R_{YA} dependences of the crystalline fractions X_C of the Si films deposited at 430 °C on the ethanol-rinsed and DIW-rinsed YSZ layers. Squares and triangles indicate the ethanol-rinse and DIW-rinse cases, respectively. Each plotted datum shows the average of 3 to 5 measurement points of one sample. The top and bottom error bars indicate the maximum and minimum values, respectively.

Fig. 3. (Color online) *In situ* RHEED patterns of the (a) bare YSZ layer at 430 °C and (b) 1-nm-thick, (c) 10-nm-thick, and (d) 60-nm-thick Si films deposited on the DIW-rinsed YSZ layers with R_{YA} = 0.13 at T_S = 430 °C. The patterns were taken sequentially during the Si film deposition. As a reference, (e) shows a pattern from an amorphous Si film.

Fig. 4. (Color online) Cross-sectional TEM images of the Si film deposited at T_S = 430 °C on the DIW-rinsed YSZ layer with R_{YA}= 0.21, where (a) is a low resolution and (b) is a high resolution (HR). The HR-TEM image (b) shows a close-up image of the dotted square frame around the interface in (a). The electron-diffraction patterns simulated based on the local lattice images enclosed by the white (point 1) and black (point 2) square frames are also shown. As for the local areas labeled as points 1 to 4, please refer to the main text.

Fig. 5. (Color online) (a) XPS survey spectra from the (i) as-deposited, (ii) HF-dipped, and

(iii) DIW-rinsed YSZ layers. The R_{YA} of the YSZ layers is 0.13. The notable points indicate the differences in the peak intensities of F and Y among the three spectra.

Fig. 6. (Color online) (a) Dependences of the Y content ratios of the chemically treated YSZ layers, R_{YC}, on R_{YA}. (b) Dependences of the F ratios of F/(Zr+Y) = R_F on R_{YA}. The chemical treatment used were the HF dipping process, the ethanol rinsing process after the HF dipping process, and the DIW rinsing process after the HF dipping process.

Fig. 7. (Color online) Concentration depth profiles of (a) Zr and Y, and (b) O and F in the 120-nm-thick Si film deposited on the ethanol-rinsed YSZ layer, and (c) O and F in the 60-nm-thick Si film deposited on the DIW-rinsed YSZ layer. They were measured by SIMS. As a reference, the Si secondary ion intensity is shown in each figure. The deposition temperature was 430 °C and the R_{YA} values for (a) and (b), and (c) were 0.08 and 0.16, respectively.

Fig. 8. (Color online) Deposition temperature dependences of the Si crystalline fractions for ethanol-rinse case. Closed and open squares indicate the results for the Si films deposited on the ethanol-rinsed YSZ layers with $R_{YA} \gtrsim 0.13$ and on the ethanol-rinsed glass substrates, respectively.

Fig. 9. (Color online) SEM images of the Secco-etched Si films deposited on the ethanol-rinsed YSZ layers at T_S = (a) 320, (b) 350, and (c) 430 °C, where the samples are the same as those in Fig. 8. In (c), the hole indicated by an arrow was formed by Secco-etching a local amorphous region.

Fig. 10. (Color online) (a) Narrow-scan XPS spectra of the Zr 3*d* from the DIW-rinsed YSZ layers with the high R_{YA} = 0.21 and low R_{YA} = 0.07. The RHEED pattern in the upper right was taken from the DIW-rinsed YSZ layer with R_{YA} = 0.07 at 430 °C just before the Si film deposition. (b) Narrow-scan XPS spectra of the Y 3*d* from the DIW-rinsed YSZ layers with the high R_{YA} = 0.21 and low R_{YA} = 0.07, and from the ethanol-rinsed YSZ layer with the low R_{YA} = 0.06. For comparison, the Zr 3*d* and Y 3*d* spectra of the as-deposited YSZ layer with R_{YA} = 0.21 are shown in (a) and (b), respectively.

Fig. 11. (Color online) Schematic model of crystallization mechanism of the Si films deposited on the ethanol-rinsed YSZ layers with the high and low R_{YA}, and on the DIW-rinsed YSZ layers with the high and low R_{YA}.

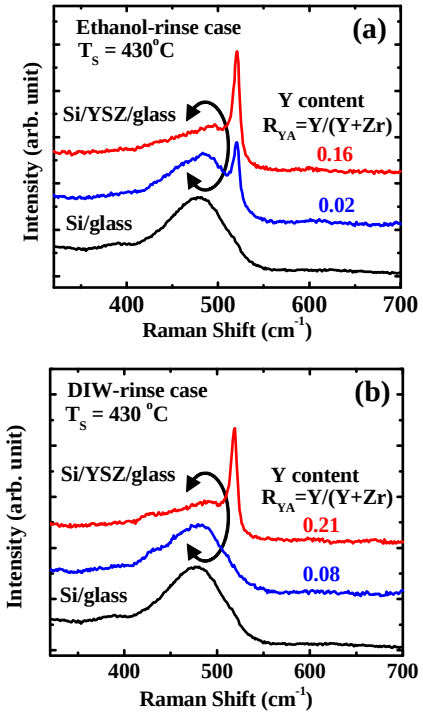

Fig. 1 **JJAP, S. Horita et al.**

1

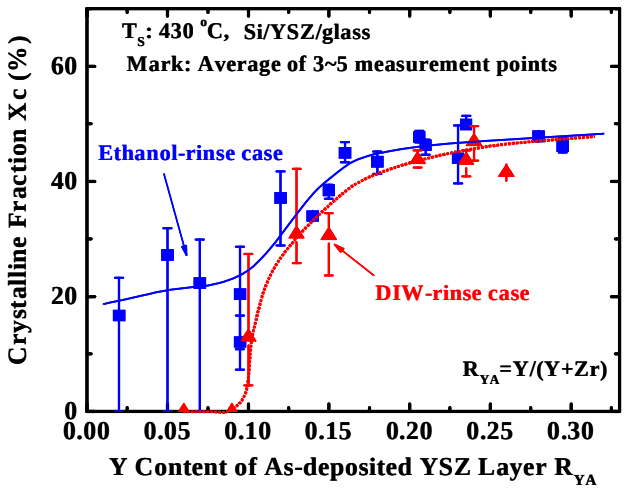

Fig. 2 **JJAP, S. Horita et al.**

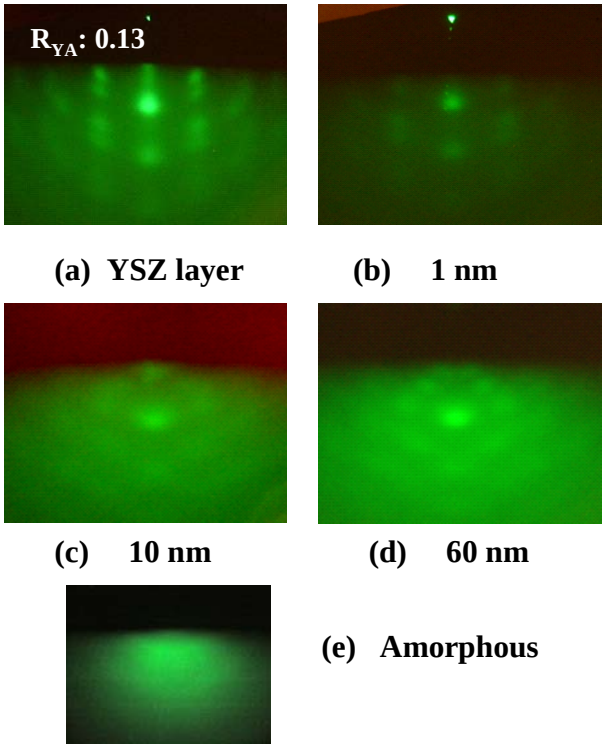

Fig. 3 **JJAP, S. Horita et al.**

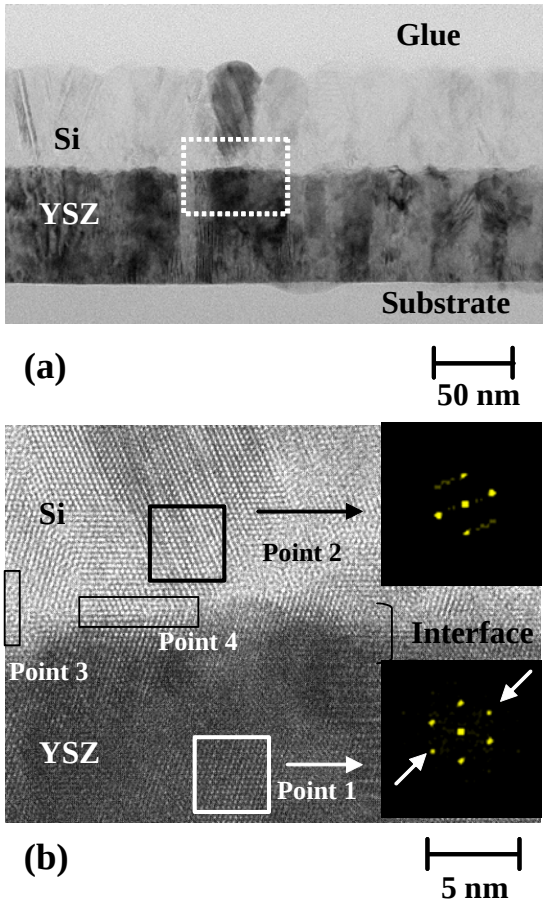

Fig. 4 **JJAP, S. Horita et al.**

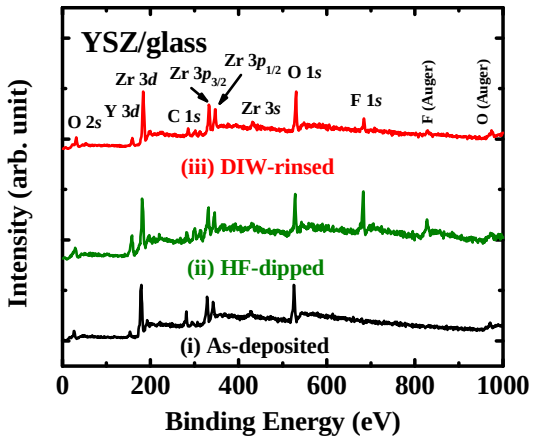

Fig. 5 **JJAP, S. Horita et al.**

5

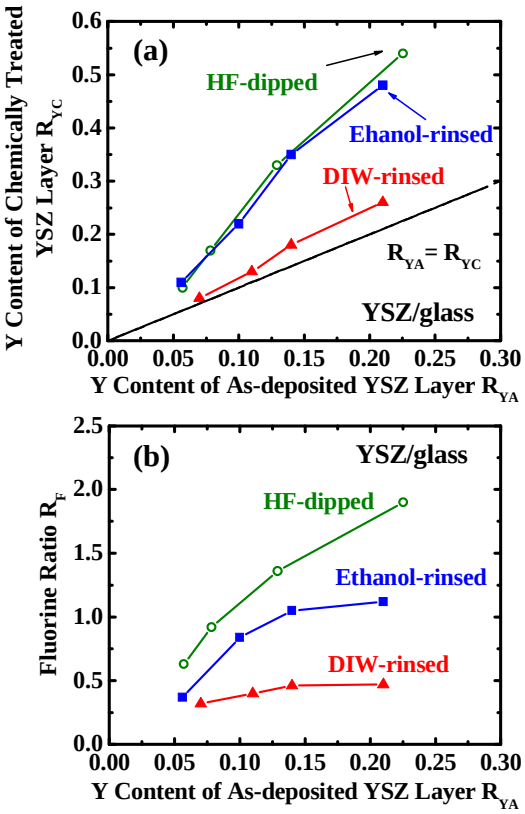

Fig. 6 **JJAP, S. Horita et al.**

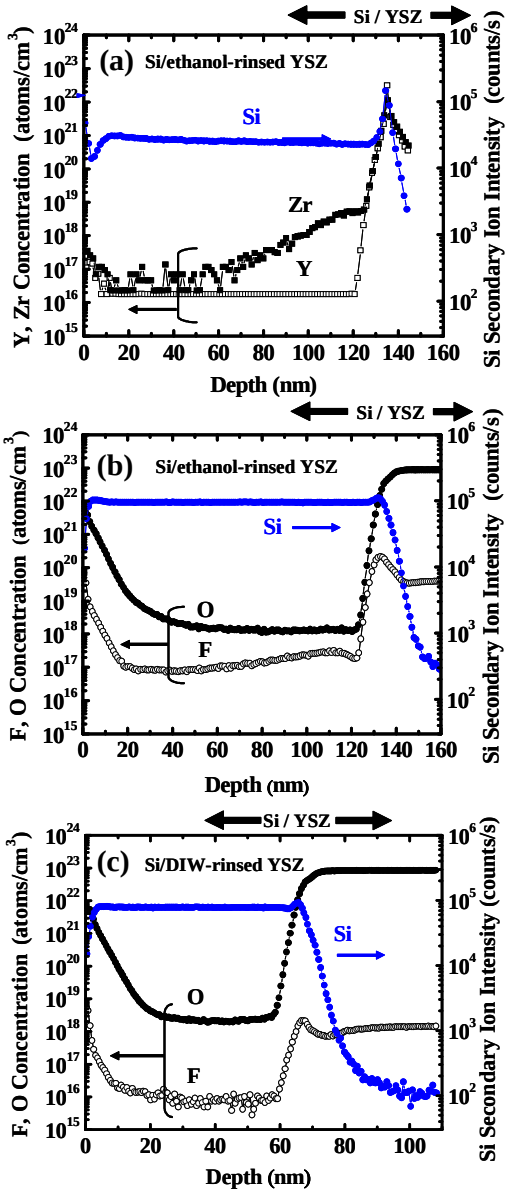

Fig. 7 **JJAP, S. Horita et al.**

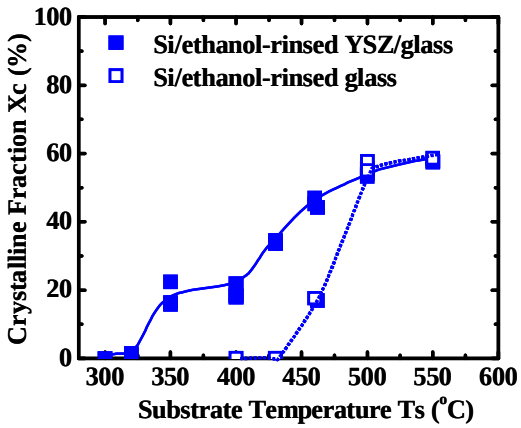

Fig. 8 **JJAP, S. Horita et al.**

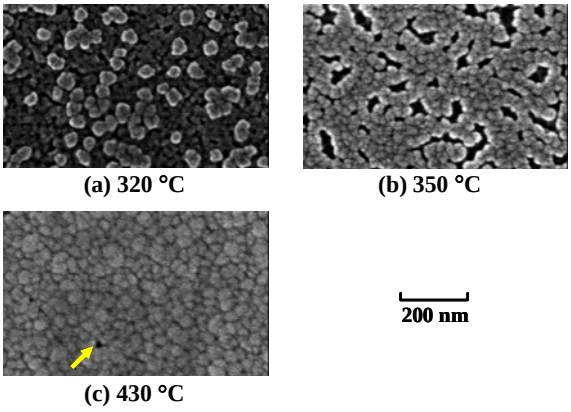

Fig. 9 **JJAP, S. Horita et al.**

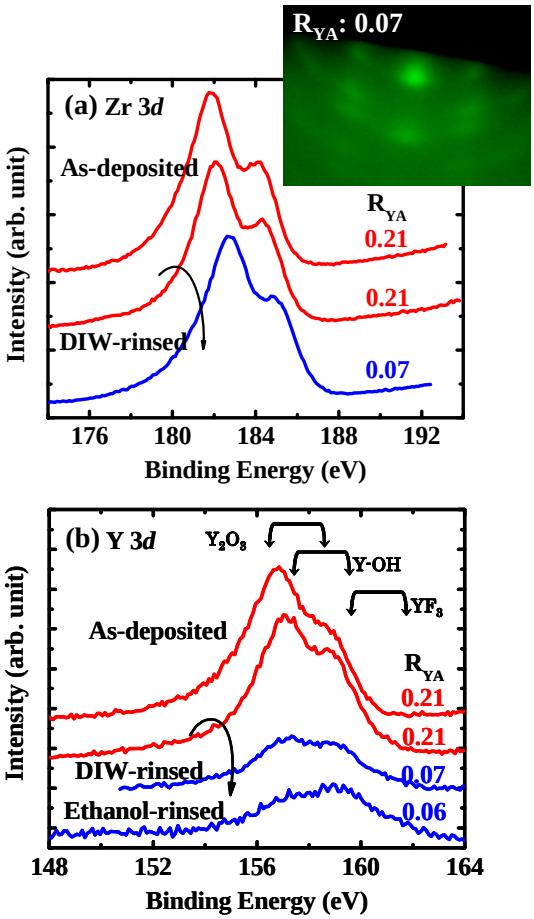

Fig. 10 **JJAP, S. Horita et al.**

1

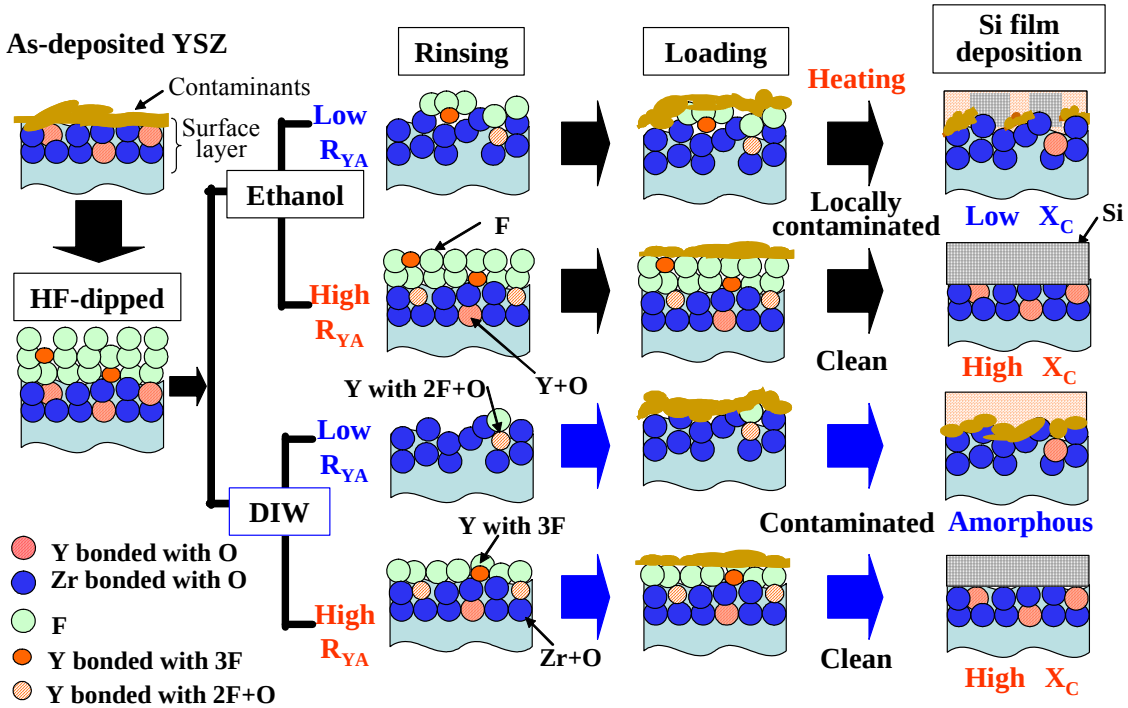

Fig. 11 **JJAP, S. Horita et al.**